

Journal of Materials Chemistry C

Accepted Manuscript



This is an *Accepted Manuscript*, which has been through the Royal Society of Chemistry peer review process and has been accepted for publication.

Accepted Manuscripts are published online shortly after acceptance, before technical editing, formatting and proof reading. Using this free service, authors can make their results available to the community, in citable form, before we publish the edited article. We will replace this *Accepted Manuscript* with the edited and formatted *Advance Article* as soon as it is available.

You can find more information about *Accepted Manuscripts* in the [Information for Authors](#).

Please note that technical editing may introduce minor changes to the text and/or graphics, which may alter content. The journal's standard [Terms & Conditions](#) and the [Ethical guidelines](#) still apply. In no event shall the Royal Society of Chemistry be held responsible for any errors or omissions in this *Accepted Manuscript* or any consequences arising from the use of any information it contains.

ZnO anchored Graphene hydrophobic nanocomposite based bulk hetero-junction solar cells showing enhanced short circuit current.

Rajni Sharma¹, Firoz Alam², A. K. Sharma³, V.Dutta², S.K.Dhawan¹

¹ CSIR-National Physical Laboratory, Dr. K. S. Krishnan Marg, New Delhi-110012, India

² Photovoltaic Laboratory, Centre for Energy Studies, Indian Institute of Technology Delhi, Hauz Khas, New Delhi 110016, India.

³ National Centre for Photovoltaic Research and Education (NCPRE), Dept. of Electrical Engineering, IIT-Bombay, Powai, Mumbai-470006, India

Abstract

Hydrophobic and surfactant free ZnO nanoparticles and ZnO decorated graphene nanocomposite (Z@G) with narrow and uniform size distribution were synthesized by time-efficient microwave assisted hydrothermal reaction specifically for application in hybrid photovoltaic. The synthesized ZnO nanoparticles and Z@G nanocomposite showed stable and clear dispersion in chloroform and methanol (with volume ratio of 9:1) & chloroform and ethanol (volume ratio 9:1), respectively. Being hydrophobic these inorganic samples blend very well with organic polymer solution in chlorobenzene which is prerequisite to cast smooth and undisrupted film for hybrid solar cell application. The introduction of these hydrophobic nanoparticles in to PCPDTBT:PCBM based bulk heterojunction polymer solar cell resulted in significant improvement in solar cell J-V characteristics with enhancement in open circuit voltage (V_{oc}), short circuit current density (J_{sc}) and thereby overall improvement in cell efficiency. With optimization of the weight ratio of polymer, fullerene and synthesized ZnO nanoparticles/Z@G nanocomposite, the power conversion efficiencies of 1.76% and 3.65% were achieved.

Keywords: A. Graphene; B. Nanoparticles; C. Nanocomposite; D. Zinc oxide; E. Hybrid solar cell; F. Short circuit current density; G. Hydrophobic.

* Corresponding author. E-mail: skdhawan@mail.nplindia.ernet.in

Fax: [+91-11-25726938](tel:+91-11-25726938); Tel: [+91-11-45609401](tel:+91-11-45609401)

Introduction

In order to compensate the continuous depleting stock of non-renewable energy resources and fulfil the emerging demand of green energy, exploitation of solar energy via photovoltaic (PV) technology is one of the most appealing solutions. Despite of high power conversion efficiency, the higher maintenance cost and expensive processing technology used in Inorganic PV (silicon based solar cells) has enforced the thinking about other cost-effective PV technology alternatives. Organic PV (conjugated polymer based organic solar cells) has succeeded in drawing the attention of researchers worldwide as being viable low cost fabrication technology, highly versatile in terms of chemical structure i.e. advanced organic chemistry, large area synthesis and most importantly eco-friendly nature. Besides the numerous favourable properties that may begin an era of lost cost PV, organic PV now is facing serious challenges in developing highly efficient polymer based devices due to bulk recombination losses and low carrier diffusion length causing less efficient charge separation and transport to respective electrodes¹⁻⁶ as well as the limitations in the device architecture.

Due to low dielectric constant value (2 to 3),⁷ the absorption of photons by conjugated polymers give rise to generation of strongly bound electron and hole pair (i.e. exciton with the binding energy ~ 400 meV) instead of free charge carriers as in case of inorganic semiconductors.⁸ Hence, in organic polymers a strong field is required to dissociate strongly bound excitons in to free electrons and holes.⁹ The low exciton diffusion length (10-15 nm) or short lifetime (hundreds of picoseconds)¹⁰ is also of major concern that ultimately contributes to the recombination losses therefore low photocurrent generation and low power conversion efficiency. Also the low charge carrier mobility (10^{-7} - 1 cm²/V.s) in organic polymers hinders the efficient charge transportation toward respective electrodes and increases the recombination losses. As per literature¹¹⁻¹⁴ most of the polymer solar cells have been reported using conjugated polymers as donor and organic fullerenes as acceptor. The fullerenes act as efficient absorber but at the same time do not contribute to the absorption being non-photoactive in nature.¹⁵ This has led to the thinking that exploiting the properties of nanostructured inorganic semiconducting materials in polymer solar cells as an acceptor may be better and to the evolution of organic/inorganic hybrid solar cells. The inorganic semiconductors contribute towards elevated photocurrent generation by the way of an improved solar spectrum absorption with tuneability of the band gap and better charge collection and transportation via high charge carrier mobility, long life time or significant diffusion length.

Zinc oxide (ZnO) qualifies as most promising inorganic semiconductor towards optoelectronic applications with its numerous useful properties like wide band gap (3.32 eV for bulk)¹⁶ that can be easily tuned by growing its nanostructures with variety of morphologies, low crystallization temperature, high chemical stability, good charge carrier mobility (to overcome charge transport limitations in organic/inorganic hybrid solar cells),¹⁷⁻¹⁹ piezoelectric nature (enhance photocurrent generation and solar to electric power conversion owing to electric field associated with polarisation induced by acoustic vibrations),²⁰ earth abundant, cheap to synthesize and non-toxic nature.²¹

Another potential material class is carbonaceous materials that finds application in various optoelectronic devices due to their attracting properties like existence in variety of nanostructures (CNT's, graphene etc.), noteworthy electrical & thermal performance parameters, abundant and eco-friendly nature.²²⁻²³ Lot of work has already been done on CNT's even regarding the application in PV but not much has happened specifically for advancement in terms of efficiency and decrement in terms of cost. Graphene with its large surface area (2600 m²/gm),²⁴ high carrier mobility (2,00,000 cm²/V/sec),²⁵ excellent thermal conductivity (5,000 W/m/K),²⁶ tuneable band gap (0 to 250 meV),²⁷ fine electron acceptor, can be extremely important and even less expensive when synthesized on large scale in comparison to CNT's.²⁸⁻²⁹ Graphene sheets generally restack and form agglomerates when used as such, owing to Vander Waals interaction. To resolve this problem either surfactant can be used or anchoring of graphene sheets with nanoparticles can be done. Use of surfactants is usually not favoured in solar cell applications as they hinder the charge transport resulting in poor device performance. The 2D structure of graphene provides a scaffold to anchor metallic and semiconducting nanoparticles and thus to develop various hybrid assemblies.³⁰ Graphene's capability to interact with excited states of semiconducting nanoparticles and undergo charge transfer by monitoring the emission life time of ZnO nanoparticles-Graphene (Inorganic-Organic) composite based samples is already reported in literature.³¹ The crystal structure of graphene is 2D hexagonal and ZnO exists in hexagonal wurtzite form, thus there is very good lattice compatibility between the two.³² Specifically its ZnO that absorb photons and generates photoelectrons, graphene only helps in conduction of these electrons. Moreover, improvement in charge transfer in Z@G nanocomposite rather than pure ZnO has already been reported.³³ This effective electron transfer from ZnO nanoparticles to graphene lower the recombination of charge carrier that ultimately improves the solar cell performance.

Microwave assisted hydrothermal route is a prime choice for synthesis of ZnO nanoparticles and graphene based composites as it affords time effectiveness in a one- step reaction (reaction time can be shortened by adjusting power, pressure and temperature of the reaction) and yields uniform morphology, small sized particles with a narrow size distribution .³⁴⁻³⁵ Also for successful synthesis of ZnO-Graphene (Z@G) nanocomposite, an effective interfacing between ZnO nanoparticles and graphene sheets without deteriorating their properties is vital. Hydrothermal route is therefore preferred for preserving the structural and electrical properties of the individual components.³⁶

Already lot of work has been done on ZnO based devices where many researchers replaced fullerenes completely by ZnO (synthesized ex-situ or in-situ, rod shaped or tetrapod) as an electron acceptor without much significant results being obtained.³⁷⁻³⁸ Additionally ZnO-graphene has been used as electron acceptor with P3HT³⁹ reporting PCE of 0.98% and also as a buffer layer in inverted solar cell³³ with enhanced efficiency of 4.15%. The novelty of our work lies on the surfactant free synthesis of hydrophobic ZnO nanoparticles (and ZnO-graphene nanocomposite) for better charge transportation in polymer solar cell. The hydrophobic nature (soluble and stable in non polar solvents like chloroform, chlorobenzene) of ZnO nanoparticles helps in casting of a smooth and continuous film for hybrid solar cell application. After successful synthesis of ZnO nanoparticles, ZnO-graphene (Z@G) nanocomposite is also worked upon using reduced Graphene oxide (RGO) as a precursor. Microwave assisted route is very significant for the reduction of RGO. Additionally the hydrophobic nature of both ZnO and graphene doesn't require any modification on graphene surface (via surfactants) to anchor ZnO nanoparticles over graphene sheet.⁴⁰ We can then use these ZnO nanoparticles and Z@G nanocomposite to fabricate hybrid solar cell. Graphene and PCBM both are different forms of carbon thus expected to form hybrid that may further improve charge conduction. Thus, instead of using these nanoparticles or nanocomposites as replacement, we use them as a supplement in PCPDTBT:PCBM based conventional type (non-inverted) solar cell.

Experimental procedure

The chemicals used in the synthesis of ZnO nanoparticles and ZnO decorated graphene nanocomposites are zinc acetate dehydrate, potassium hydroxide, methanol from Merck,

India and RGO was procured from ACS Materials. Monowave 300 (Anton Paar) microwave reactor was used for the above synthesis of nanoparticles and nanocomposite.

Synthesis of Hydrophobic ZnO nanoparticles

0.6 gm of Zinc acetate was dissolved in 20 ml of methanol and 10 ml distilled water at 60⁰ C. Then a solution of 0.3 gm of Potassium hydroxide in 13 ml of methanol was added with stirring for 10-15 minutes to obtain a clear solution. 25 ml of final solution was poured into 30 ml glass tube tightened with septum and finally placed in Teflon lined microwave reactor. The reaction was carried out at 160⁰ C for half an hour and then the reactor was cooled down to 55⁰ C to obtain a milky white solution. Keep the solution untouched for 20 minutes so that the precipitates may settle down. The obtained precipitates were washed and centrifuged at 8,000 rpm 3-4 times, followed by annealing at 100⁰C for half an hour to get pure ZnO nanoparticles. The process steps captured at various stages are also shown in Fig. 1. Additionally the variation of pressure, temperature and power during reaction has been given as S1 in supplementary information along with hydrophobic evaluation as S3. The clear and stable dispersion of ZnO nanoparticles was obtained in the mixture of chloroform and methanol (with volume ratio 9:1).

Synthesis of ZnO nanoparticles decorated Graphene (or Z@G) nanocomposite

ZnO nanoparticles decorated graphene was synthesized by the hydrothermal reaction in a microwave reactor. A solution of RGO in ethanol was prepared by adding 5 mg of commercial (ACS materials) RGO in 10 ml of ethanol and ultrasonicated for 10-15 minutes. In a separate beaker another solution was prepared by dissolving 0.6 gm of Zinc acetate dehydrate in 20 ml of methanol and 10 ml dist. water at 60⁰ C, followed by addition of 0.3 gm of KOH dissolved in 13 ml of methanol with stirring for 10-15 minutes. RGO solution was added to the zinc precursor and again ultrasonicated for 10 minutes. 25 ml of the final solution was poured in to a glass tube having total capacity of 30ml and was tightened with septum and placed in a Teflon lined reactor. The reaction was carried out at 160⁰ C for an hour and finally cooled down to 55⁰ C. After completion of reaction greyish colour precipitates obtained were washed and centrifuged at 10,000 rpm 3-4 times and finally annealed at 100⁰C for half an hour to obtain ZnO decorated graphene nanocomposite (Z@G). Fig. 2 illustrates the process steps for preparing the ZnO decorated graphene nanocomposite. The graph showing variation of temperature, pressure and power during reaction is shown as

S2 in supplementary information. The stable suspension was obtained in a mixture of chloroform and ethanol (with volume ratio 9:1).

Characterization of ZnO nanoparticles and ZnO decorated graphene (Z@G) nanocomposite

In order to investigate the particle size and micro structural properties of the synthesized ZnO nanoparticles and Z@G nanocomposite, Transmission electron microscopy (TEM) and high-resolution transmission electron microscopy (HRTEM) measurements were performed using Tecnai G2 F30 S-Twin instrument operating at 300KV as accelerating voltage using a drop cast sample dispersed in chloroform on to a carbon coated copper grid. Shimadzu UV-1601 spectrophotometer was used to record absorption spectra. Photoluminescence spectra were acquired using Perkin Elmer LF55 having xenon source spectrophotometer (in the wavelength region of 320-500 nm). Atomic force microscopy (AFM) studies were performed by multimode AFM with Nanoscope V controller (Veeco, USA) in tapping mode. Fourier transform infrared analysis (FTIR) was carried out using Nicolet 5700 in transmission mode in wave number range 400 – 4000 cm^{-1} to determine the functional groups present in the synthesized samples. Crystal structure and phase analysis was done by using D8-Advance XRD (Bruker) using Cu $K\alpha$ radiation (wavelength, $\lambda = 1.54 \text{ \AA}$) in the scattering range (2θ) of 10^0 to 80^0 with a scan rate of $0.02^0/\text{sec}$ and slit width of 0.1 mm. Raman scattering was performed by using Renishaw in Via Reflex spectrometer (UK) with an excitation source at 514.5 nm having resolution less than 1.0 cm^{-1} . To calculate the Hydrophobicity of synthesized ZnO nanoparticles, Contact angles were recorded on Drop Shape Analysis System DSA10MK2 from Krüss GmbH, Germany.

Hybrid solar cell fabrication and characterization:

ZnO nanoparticles and ZnO decorated graphene nanocomposite (Z@G) based bulk heterojunction solar cells (ITO/PEDOT:PSS/PCPDTBT:PCBM:ZnO (or Z@G) /Al) with an active area of 0.1 cm^2) were fabricated by varying the concentration of PCPDTBT: PCBM: ZnO (or Z@G) and also by varying the weight ratio of the polymer, fullerene and nanoparticles. The solution of the polymer, fullerene and ZnO (or Z@G) in chlorobenzene was spin coated as an active layer on ITO coated glass substrate of sheet resistance 10-14 Ω -

cm⁻¹ with poly(ethylenedioxythiophene) : poly(styrene sulfonic acid) (PEDOT:PSS) coating as the buffer layer. Here ITO acts as bottom electrode. PEDOT:PSS coating was done at 2,000 rpm whereas active layer was spin coated at 800 rpm under ambient condition. Finally, 100 nm thick Aluminium (Al) was deposited by thermal evaporation unit through a shadow mask at 2×10^{-6} Torr as top metal contact of the device.

The performance of polymer bulk heterojunction solar cells fabricated with ZnO nanoparticles and ZnO decorated Graphene nanocomposite (Z@G) was evaluated with the current density-voltage (J-V) characteristics measured with class AAA solar simulator (sol3A Oriel Newport USA) equipped with xenon lamp used as light source under standard test conditions (STC).

Result and Discussion

Structural and morphological investigations:

The XRD spectra for reduced graphene oxide (RGO), ZnO nanoparticles (ZnO) and ZnO-graphene nanocomposite (Z@G) are shown in Fig. 3 to analyze the phase and crystallinity of ZnO and RGO along with the interlayer effect in hybrid or composite. A broad band of (002) peak of graphite at $2\theta = 29.37^\circ$ is observed in RGO which corresponds to d-spacing of 0.31 nm. The reason for small d- value lies in aggregation of the reduced graphene sheets due to weak Vander Waals force of attraction between nanosheets.⁴¹ The XRD pattern of ZnO nanoparticles shows the reflections (100), (002), (101), (102), (110), (103), (112), (004) and (202) of ZnO in a hexagonal Wurtzite lattice.⁴² The absence of any secondary phase confirms the synthesis of pure and single phase ZnO nanoparticles. In addition, small sized ZnO nanoparticles are directly evidenced from the broad peaks. The calculated average crystallite size using Scherrer's equation for ZnO sample comes out to be 4.5 nm whereas for Z@G nanocomposite the evaluated crystallite size is around 8 nm. In Z@G XRD pattern, no diffraction peak corresponding to RGO was observed. It can be explained in two ways – (i) lesser amount, giving relatively low diffraction intensity of RGO than ZnO in the Z@G nanocomposite and (ii) anchoring of ZnO nanoparticles on RGO may inhibit the restacking of carbon sheets, which results in weak diffraction peak or no diffraction peak at all.^{43,44}

The morphological analysis of synthesized ZnO nanoparticles and Z@G nanocomposite hetero structure using high resolution transmission electron microscopy (HRTEM) is given in

Fig. 4. The HRTEM image of ZnO sample shown in Fig. 4 (a) clearly illustrates the quasi spherical ZnO nanoparticles in the range 4-8 nm with average size 5.25 nm as depicted in the histogram. Fig 4 (b) shows the image at higher resolution and selected area electron diffraction (SAED) pattern in the inset. The SAED pattern provides a clear evidence of the highly crystalline ZnO structure with all diffraction rings being indexed to hexagonal Wurtzite phase of ZnO. This observation supports well the synthesis of phase pure ZnO nanoparticles via the time efficient hydrothermal method. The lattice fringes encircled image shown in Fig. 4 (b) gives an inter-planar distance of 0.28 nm that can be assigned to (100) plane of hexagonal ZnO. Fig. 4 (c) illustrates the ZnO nanoparticles-Graphene nanocomposite (Z@G) images having ZnO nanoparticles with nearly spherical symmetry & narrow size distribution in the range 3-11 nm anchored on graphene sheet. The average size of ZnO nanoparticles decorated on graphene sheet is ~ 7 nm from the histogram. The enhancement in the average size of ZnO nanoparticles from 5.25 nm to 7 nm with the introduction of graphene is probably due to longer duration of anneal time (30 min. to 60 min.) that results in the growth of ZnO nanoparticles. Also, an intimate contact between ZnO nanoparticles and graphene can be witnessed from HRTEM image shown in Fig 4 (c). This intimate contact will provide proper electronic interaction between Graphene & ZnO nanoparticles that is very much required to have better charge separation (or less charge carrier recombination)⁴⁵, therefore crucial for improvement in power conversion efficiency of hybrid solar cells. The high magnification image corresponding to Z@G nanocomposite, elaborated in SAED pattern taken for the encircled fringes, is shown in Fig. 4(d). The polycrystalline nature of Z@G nanocomposite is evidenced from SAED pattern.

Optical investigations:

The absorption spectra of as synthesized ZnO nanoparticles and Z@G nanocomposite are shown in Fig. 5. It is clearly observed that in pure ZnO, a strong absorption peak at 364 nm, having corresponding band gap of 3.4 eV, is at a lower wavelength (blue shifted) than that for bulk ZnO (corresponding to 3.32 eV) as per literature.¹⁶ This blue shift is due to the synthesis of small-sized ZnO nanoparticles via the facile and simple hydrothermal method. In addition the sharp characteristic absorption peak clearly points to the good crystallinity and high purity of synthesized ZnO nanoparticles. The Z@G nanocomposite shows an absorption peak at 372 nm. The possible reason for this red shift may lie in: (1) the nanocomposite structure which may favour the prominent absorption of ZnO rather than that of graphene (2)

coupling between ZnO and graphene (3) the increased particle size in Z@G (i.e. 8-10 nm) than pure ZnO (i.e. 4-5 nm), as evident from XRD spectra shown in Fig. 3.

The optical properties of the synthesized ZnO nanoparticles and Z@G nanocomposite samples were also monitored using photoluminescence (PL) spectroscopy as shown in fig. 6. The PL spectrum of pure ZnO nanoparticles shows a UV emission band centred at 385 nm (3.22 eV) which is related to recombination of excitons.⁴⁶ Also, the absence of emission band in the wavelength range 500 – 600 nm signifies defect free, excellent quality ZnO nanoparticles.⁴⁷ In comparison, the PL peak position of Z@G nanocomposite shows a red shift to 391 nm (3.17 eV). The shift in the PL emission of Z@G composite might be due to interaction in between ZnO nanoparticles and graphene.

FTIR and Raman analysis:

In order to find out the functional groups attached with ZnO nanoparticles & RGO and also for the identification of chemical changes in RGO due to anchoring of ZnO nanoparticles (Z@G) the Fourier transform infrared (FTIR) spectroscopy was done (Fig. 7). The broad peak in the range of 3500 – 3300 cm^{-1} corresponds to the OH stretching vibration in pure ZnO whereas the peak at 1406 cm^{-1} shows OH bending vibration. The small peaks at 917 cm^{-1} and 676 cm^{-1} clearly indicates Zn-O stretching⁴⁸ while the peaks at 1584 cm^{-1} and 1020 cm^{-1} are attributed to C-O stretching vibration and unreacted acetate left after reaction. Now in the RGO plot, the most intense peak at 1165 cm^{-1} shows the presence of C-O stretching vibration and the second most intense peak at 1545 cm^{-1} is due to skeletal in plane vibration of C=C.⁴⁹ The peaks in the range 2920 cm^{-1} to 2850 cm^{-1} is due to asymmetric C-H stretching, also small peak positioned at 1736 cm^{-1} shows stretching vibration from C=O.⁵⁰ In the Z@G nanocomposite plot, intensity of peak at 1557 cm^{-1} gets maximized which is due to skeletal in plane vibration of C=C whereas it is less pronounced in RGO data which is a clear indication of a further reduction of RGO in to graphene. This is further supported by weakened oxygen related peaks in Z@G nanocomposite at 2365 cm^{-1} and 1013 cm^{-1} than those in RGO which simply means deoxygenation of RGO toward graphene during Z@G nanocomposite formation. The peaks at 655 cm^{-1} and 920 cm^{-1} are due to Zn-O stretching, indicating anchoring of ZnO on graphene sheet.⁴⁸

Raman spectroscopy being non-destructive is one of the most widely used techniques to investigate order and disorder specifically in carbon based materials. The Raman spectra of commercial RGO and hydrothermally synthesized Z@G nanocomposite are shown in fig 8. Both the samples have the characteristic D-band (1349 and 1353 cm^{-1}) and G-band (1593 and 1597 cm^{-1}) respectively; D-band being assigned to local defects and disorders whereas G-band originates from symmetric stretching of sp^2 C-C bond.⁵¹ It can be clearly noticed that the D-band of the Z@G nanocomposite is blue shifted by 4cm^{-1} while G-band is red shifted again by 4cm^{-1} in comparison to RGO. These shifts indicate the interaction between graphene and ZnO nanoparticles which is a prerequisite for charge transfer between ZnO and graphene.⁵² In addition, the low intensity ratio (I_D/I_G) of D to G-band (0.857 and 0.868) for RGO and Z@G nanocomposite, respectively, suggests creation of very less defects in nanocomposite on introduction of ZnO nanoparticles.

Hybrid solar cell Characterization:

In order to develop efficient polymer based solar cells most of the attention has been paid towards donor part (i.e. conjugated polymers) whereas very less work has been done in the direction of acceptor part (i.e. fullerenes). Some work has been reported by replacing organic fullerenes by inorganic semiconducting acceptors but results are not much significant.^{37,40,53} Instead of total replacement of organic fullerenes we have deployed synthesized inorganic nanostructured materials as supplementary acceptor along with organic fullerenes. In this way we not only exploit the organic blend of polymer:fullerene (PCPDTBT: PCBM) for effective exciton dissociation at the favourable organic: organic interface rather than organic: inorganic interface, but also at the same time have the advantage of lowering the overall volume of costly organic blend by supplementing with inexpensive ZnO nanoparticles (or Z@G nanocomposite). Additionally due to higher charge mobility along with conducting pathways provided by inorganic semiconductors, the charge carriers will get extracted rapidly that ultimately leads to lower recombination. In this manner we not only bring down the fabrication cost of polymer based devices but also achieve better open circuit voltage (V_{OC}) and short circuit current density (J_{SC}) values.

The solar cell devices were fabricated with overall concentration 30 mg/ml and 40 mg/ml (PCPDTBT: PCBM: ZnO nanoparticles {or Z@G} in chlorobenzene) of active layer and different weight ratios as 1:1:1 & 1:1:2 of PCPDTBT:PCBM:ZnO/Z@G and the

corresponding J-V characteristics are shown in Fig. 9 (a) & (b). All performance parameters of the solar cells are tabulated in Table I.

The best efficiency devices (Z-3 and ZG-3) have the weight ratio of 1:1:1 (PCPDTBT:PCBM:ZnO or Z@G) with active layer concentration of 40 mg/ml for both ZnO and Z@G nanocomposite as supplement. When measured under standard AM 1.5 G solar spectrum with power density of 100 mW-cm⁻², the best Z@G device gives an efficiency of 3.65 % with J_{SC} value 17.5 mA-cm⁻², V_{OC} 0.66 V and FF 32 %. Similarly in case of ZnO device the best efficiency achieved is 1.76 % with J_{SC} 9.5 mA-cm⁻², V_{OC} 0.59 V and FF 31 %.

It is clearly observed that by replacing ZnO nanoparticles by Z@G nanocomposite the power conversion efficiency of the device becomes more than double with doubling of the J_{SC} value. A small improvement in V_{OC} along with enhanced J_{SC} value and nearly unchanged FF are observed. The probable reason for increased J_{sc} is the larger specific area of graphene sheets that ultimately leads to large heterojunction interface with polymer matrix for efficient exciton separation, and the ability of graphene to interact with excited ZnO decorated over graphene sheet followed by capturing and transportation of charge carriers toward respective electrodes.^{24,31,35,45,52} The PL quenching data shown in S4 (supplementary information) clearly indicates the charge transfer between the polymer and ZnO nanoparticles (or Z@G nanocomposite).

When the devices are fabricated using Z@G nanocomposite at overall concentration of 40 mg/ml but with increased weight proportion of Z@G i.e. 1:1:2 (PCPDTBT:PCBM:Z@G) the efficiency gets reduced to 3.18 % with J_{SC} value lowered to 13.6 mA/cm² and a bit increment in V_{OC} to 0.71 V (due to higher content of wide band gap ZnO that ultimately affects the open circuit voltage rather than short circuit current density). The increment in open circuit voltage is not compensated by the large decrement in short circuit current density. This is due to the aggregation of Z@G in polymer matrix on increasing the amount of nanocomposite that will ruin the film homogeneity and ultimately gives rise to a disrupted active layer⁵⁴ with inefficient charge transport. In the similar manner we may explain the decrease in efficiency of ZnO based devices on increasing the ZnO nanoparticle content.

Additionally ZnO and Z@G based devices (Z-1, ZG-1) prepared with overall concentration of 30 mg/ml of active layer give comparatively less efficiency (0.68 %, 2.16 %) than the devices (Z-3, ZG-3) prepared with concentration 40 mg/ml. Thickness of the

active layer may be probable reason for this; thicker the active layer more will be the generation of excitons by the enhanced absorption of photons.⁵⁵

From the AFM images shown in Fig. 10 (a) & (b), it is very clear that ZnO particles owing to its hydrophobic nature form a very uniform film with PCPDTBT and PCBM and the low roughness value of 0.325 nm indicates the quality of active layer for hybrid solar cell device fabrication. The AFM images obtained for ZnO decorated graphene shows some different but interesting pattern in the film. The probable reason for higher efficiency of Z@G nanocomposite based devices may evolve from this uniform pattern. These flake shaped surface structure may arise due to hybridization of C-60 compound and graphene sheet as both belongs to one or the other form of nanocarbon thus having no interfacial issues and moreover the strong affinity between C-60 and carbon allotrope justifies the hybrid formation.⁵⁶ Such pattern favours the transportation of charge carriers thus leads to lower recombination losses and ultimately results in higher efficiency of devices.

In order to further probe the nature of enhancement in J_{SC} , external quantum efficiency (EQE) of cell having ZnO and Z@G has been done. Fig. 11 represents sharp features in the EQE spectrum of ZnO nanoparticles (or Z@G nanocomposite) blended with PCPDTBT:PCBM. The region centred at 730 nm is dominated by PCPDTBT contribution while the other one centred at 410 nm can be assigned to ZnO (or Z@G) and PCBM superposition.^{57,58} EQE as high as 26% at maximum peak has been achieved in ZnO based devices whereas for Z@G, EQE value jumps to 65%. This is in accordance with the J_{SC} value obtained from I-V curves for ZnO and Z@G based devices (Fig. 9). The prominent increase in EQE for Z@G based device demonstrates improved charge transfer that ultimately result in enhanced short circuit current density. The densely packed ZnO nanoparticles on graphene sheet generate photoelectrons and have been effectively transferred to graphene. This will suppress the recombination of charge carriers and enhance transportation of charge carriers toward respective electrodes that ultimately results in increased short circuit current density.

On comparing devices made up of ZnO and Z@G nanocomposite, we clearly observe significant enhancement in short-circuit current (J_{sc}) and thus improvement in overall efficiency in Z@G nanocomposite based devices. Still we need to work on the fabrication of devices so as to overcome the losses due to series and shunt resistance to get better results.

Conclusion

In conclusion, hydrophobic ZnO nanoparticles (ZnO) and ZnO decorated graphene nanocomposite (Z@G) are synthesized via simple and time-efficient microwave assisted hydrothermal method without using any surfactant. ZnO and Z@G show good solubility in chlorobenzene and this result in a very smooth and uniform film with polymer and fullerene blend. The power conversion efficiency of PCPDTBT:PCBM:Z@G based devices show significant enhancement than the PCPDTBT:PCBM:ZnO based devices. The best performance devices (Z-3 and ZG-3) are obtained at weight ratio of 1:1:1 (PCPDTBT:PCBM:ZnO {or Z@G}) with overall active layer concentration of 40 mg/ml for both ZnO and Z@G nanocomposite as supplement in polymer based bulk hetero junction solar cells. The best efficiency achieved in ZnO based device is 1.76 % with J_{SC} 9.53 mA-cm⁻², V_{OC} 0.59 V and FF being 31 % whereas by replacing ZnO with Z@G the efficiency increases to 3.65% (i.e. more than the double) with J_{SC} value 17.45 mA-cm⁻², V_{OC} being 0.66 V and FF of 32 %. This clearly shows the significant impact of graphene on improved polymer solar cell performance through better charge transportation.

Acknowledgement

The authors would like to thank Director, National Physical Laboratory, CSIR, New Delhi for providing material synthesis and their characterization facility. We gratefully acknowledge Indian Institute of Technology Delhi (IITD), for facilitating solar cell device fabrication and characterization. One of the authors Rajni Sharma is thankful to CSIR for providing SRF to carry out the research work for completion of her doctorate.

Reference(s):

1. F. C. Krebs, *Sol. Energy Mater. Sol. Cells*, 2009, **93**, 394–412.
2. U. Zhokhavets, T. Erb, G. Gobsch, M. Al-Ibrahim, O. Ambacher, *Chem. Phys. Lett.*, 2006, **418**, 347–350.
3. H. Y. Chen, J. Hou, S. Zhang, Y. Liang, G. Yang, Y. Yang, L. Yu, Y. Wu, G. Li, *Nat. Photonics*, 2009, **3**, 649–653.
4. M. A. Green, K. Emery, Y. Hishikawa, W. Warta, E. D. Dunlop, *Progr. Photovolt.: Res. Appl.*, 2012, **20**, 12–20.
5. S. H. Park, A. Roy, S. Beaupre, S. Cho, N. Coates, J. S. Moon, D. Moses, M. Leclerc, K. Lee, A. J. Heeger, *Nat. Photonics*, 2009, **3**, 297–302.
6. A. A. Bakulin, A. Rao, V. G. Pavelyev, P. H. M. van Loosdrecht, M. S. Pshenichnikov, D. Niedzialek, J. Cornil, D. Beljonne, R. H. Friend, *Science*, 2012, **335**, 1340–1344.
7. W. Cai, X. Gong, Y. Cao, *Sol. Energy Mater. Sol. Cells*, 2010, **94**, 114–127.
8. S. C. J. Meskers, J. Hubner, M. Oestreich, H. Baessler, *J. Phys. Chem. B*, 2001, **105**, 9139-9149.
9. P. B. Miranda, D. Moses, A. J. Heeger, *Phys. Rev. B*, 2001, **64**, 812011-812014.
10. T. J. Savenije, J. M. Warman, A. Goossens, *Chem. Phys. Lett.*, 1998, **287**, 148-153.
11. K. M. Coakley, M. D. McGehee, *Chem. Mater.*, 2004, **16**, 4533-4542.
12. S. Gunes, H. Neugebauer, N. S. Sariciftci, *Chem. Rev.*, 2007, **107**, 1324-1338.
13. A. Moliton, J. M. Nunzi, *Polym. Int.*, 2006, **55**, 583-600.
14. B. R. Saunders, M. L. Turner, *Adv. Colloid Interface Sci.*, 2008, **138**, 1-23.
15. M. Skompska, *Synth. Met.*, 2010, **160**, 1–15.
16. Ü. Özgür, Y. I. Alivov, C. Liu, A. Teke, M. A. Reshchikov, S. Doğan, V. Avrutin, S.J. Cho, and H. Morkoç, *J. App. Phys.*, 2005, **98**, 041301-041404.
17. S. D. Oosterhout, M. M. Wienk, S. S. van Bavel, R. Thiedmann, L. J. A. Koster, J. Gilot, J. Loos, V. Schmidt and R. A. J. Janssen, *Nat. Mater.*, 2009, **8**, 818-824.
18. S. Shao, K. Zheng, K. Zidek, P. Chabera, T. Pullerits and F. Zhang, *Sol. Energy Mater. Sol. Cells*, 2013, **118**, 43–47.
19. Z. R. Tian, J. A. Voigt, J. Liu, B. Mckenzie, M. J. Mcdermott, M. A. Rodriguez, H. Konishi, H. Xu, *Nat. Mater.*, 2003, **2**, 821-826.
20. S. Shoaee, J. Briscoe, J. R. Durrant and S. Dunn, *Adv. Mater.*, 2013, **26**, 263-268.
21. J. Zhou, N. S. Xu and Z. L. Wang, *Adv. Mater.*, 2006, **18**, 2432–2435.

22. N. M. Gabor, Z. Zhong, K. Bosnick, J. Park, P. L. McEuen, *Science*, 2009, **325**, 1367-1371.
23. B. Farrow, P. V. Kamat, *J. Am. Chem. Soc.*, 2009, **131**, 11124-11131.
24. S. Stankovich, D. A. Dikin, G. H. B. Dommett, K. M. Kohlhaas, E. J. Zimney, E. A. Stach, R. D. Piner, S. T. Nguyen, R. S. Ruoff, *Nature*, 2006, **442**, 282-286.
25. K. I. Bolotin, K. J. Sikes, Z. Jiang, M. Klima, G. Fudenberg, J. Hone, P. Kim and H. L. Stormer, *Solid State Commun.*, 2008, **146**, 351-355.
26. A. A. Balandin, S. Ghosh, W. Bao, I. Calizo, D. Teweldebrhan, F. Miao and C. N. Lau, *Nano Lett.*, 2008, **8**, 902-907.
27. Y. Zhang, T. T. Tang, C. Girit, Z. Hao, M. C. Martin, A. Zettl, M. F. Crommie, Y. R. Shen, and F. Wang, *Nature*, 2009, **459**, 820-823.
28. Y. Xu, H. Bai, G. Lu, C. Lu, G. Shi, *J. Am. Chem. Soc.*, 2008, **130**, 5856-5857.
29. Z. F. Liu, Q. Liu, Y. Huang, Y. F. Ma, S. G. Yin, X. Y. Zhang, W. Sun and Y. S. Chen, *Adv. Mater.*, 2008, **20**, 3924-3930.
30. S. W. Tong, N. Mishra, C. L. Su, V. Nalla, W. Wu, W. Ji, J. Zhang, Y. Chan and K. P. Loh, *Adv. Funct. Mater.*, 2014, **24**, 1904-1910
31. Z. Chen, S. P. Berciaud, C. Nuckolls, T. F. Heinz, L. E. Brus, *ACS Nano*, 2010, **4**, 2964-2968.
32. A. M. Munshi, D. L. Dheeraj, V. T. Fauske, D. C. Kim, A. T. J. van Helvoort, B. O. Fimland, H. Weman, *Nano Lett.*, 2012, **12**, 4570-4576.
33. H. W. Lee, J. Y. Oh, T. Lee, W. S. Jang, Y. B. Yoo, S. S. Chae, J. H. Park, J. M. Myoung, K. M. Song and H. K. Baik, *Appl. Phys. Lett.*, 2013, **102**, 193903(1-4)
34. M. Khenfouch, M. Bai'toul, M. Maaza, *Opt. Mater.*, 2012, **34**, 1320-1326.
35. B. Saravanakumar, R. Mohan, S. J. Kim, *Mate. Res. Bull.*, 2013, **48**, 878-883.
36. H. Park, S. Chang, J. Jean, J. J. Cheng, P. T. Araujo, M. Wang, M. G. Bawendi, M. S. Dresselhaus, V. Bulović, J. Kong and S. Gradečak, *Nano Lett.*, 2013, **13**, 233-239.
37. L. Baeten, B. Conings, H. G. Boyen, J. D'Haen, A. Hardy, M. D'Olieslaeger, J. V Manca, M. K. Van Bael, *Adv. Mater.* 2011, **23**, 2802-2805.
38. D. E. Motaung, G. F. Malgas, S. S. Ray and C. J. Arendse, *Thin Solid Films*, 2013, **537**, 90-96.
39. Q. Zheng, G. Fang, F. Cheng, H. Lei, W. Wang, P. Qin and H. Zhou, *J. Phys. D: Appl. Phys.*, 2012, **45**, 455103(1-8).
40. H. Park, P. R. Brown, V. Buloyic, J. Kong, *Nano Lett.*, 2012, **12**, 133-140.

41. Y. Feng, H. Liu, W. Luo, E. Liu, N. Zhao, K. Yoshino and W. Feng, *Sci. Rep.*, 2013, **3**, 3260 (1-8).
42. S. Liu, H. Sun, A. Suvorova and S. Wang, *Chem. Eng. J.*, 2013, **229**, 533 -539.
43. C. Xu, X. Wang and J. Zhu, *J. Phys. Chem. C*, 2008, **112**, 19841–19845.
44. X. Liu, L. Pan, Q. Zhao, T. Lv, G. Zhu, T. Chen, T. Lu, Z. Sun and C. Sun, *Chem. Eng. J.*, 2012, **183**, 238-243.
45. Y. Yokomizo, S. Krishnamurthy and P. V. Kamat, *Catalysis Today*, 2013, **199**, 36-41.
46. J. M. Lee, Y. B. Pyun, J. Yi, J. W. Choung, and W. Park, *J. Phys. Chem. C*, 2009, **113**, 19134–19138.
47. H. Park, S. Chang, J. Jean, J. J. Cheng, P. T. Araujo, M. Wang, M. G. Bawendi, M. S. Dresselhaus, V. Bulović, J. Kong, and S. Gradečak, *Nano Lett.*, 2013, **13**, 233–239.
48. S. Mitra, P. Patra, S. Chandra, P. Pramanik and A. Goswami, *Appl. Nanosci.*, 2012, **2**, 231–238.
49. F. Jiang, L. W. Yang, Y. Tian, P. Yang, S. W. Hu, K. Huang, X. L. Wei and J. X. Zhong, *Ceram. Int.*, 2014, **40**, 4297–4304.
50. Yewen Cao, Zuliang Lai, Jiachun Feng and Peiyi Wu, *J. Mater. Chem.*, 2011, **21**, 9271-9278.
51. D. Graf, F. Molitor, K. Ensslin, C. Stampfer, A. Jungen, C. Hierold and L. Wirtz, *Nano Lett.*, 2007, **7**, 238-242.
52. H. Yu, T. Wang, B. Wen, M. Lu, Z. Xu, C. Zhu, Y. Chen, X. Xue, C. Sun and M. Cao, *J. Mater. Chem.*, 2012, **22**, 21679-21685.
53. B. R. Saunders, *J. Colloid Interface Sci.*, 2012, **369**, 1–15.
54. W. J. E. Beek, M. M. Wienk and R. A. J. Janssen, *Adv. Mater.*, 2004, **16**, 1009-1013.
55. W. Li, K. H. Hendriks, W. S. C. Roelofs, Y. Kim, M. M. Wienk and R. A. J. Janssen, *Adv. Mater.*, 2013, **25**, 3182–3186.
56. E. K. Jeon, C. S. Yang, Y. Shen, T. Nakanishi, D. S. Jeong, J. J. Kim, K. S. Ahn, K. J. Kong and J. O. Lee, *Nanotechnology*, 2012, **23**, 455202-455208.
57. A. R. Yusoff, H. P. Kim and J. Jang, *Nanoscale*, 2014, **6**, 1537-1544.
58. A. V. Tunc, A. D. Sio, D. Riedel, F. Deschler, E. D. Como, J. Parisi and E. V. Hauff, *Org. Elect.*, 2012, **13**, 290-296.

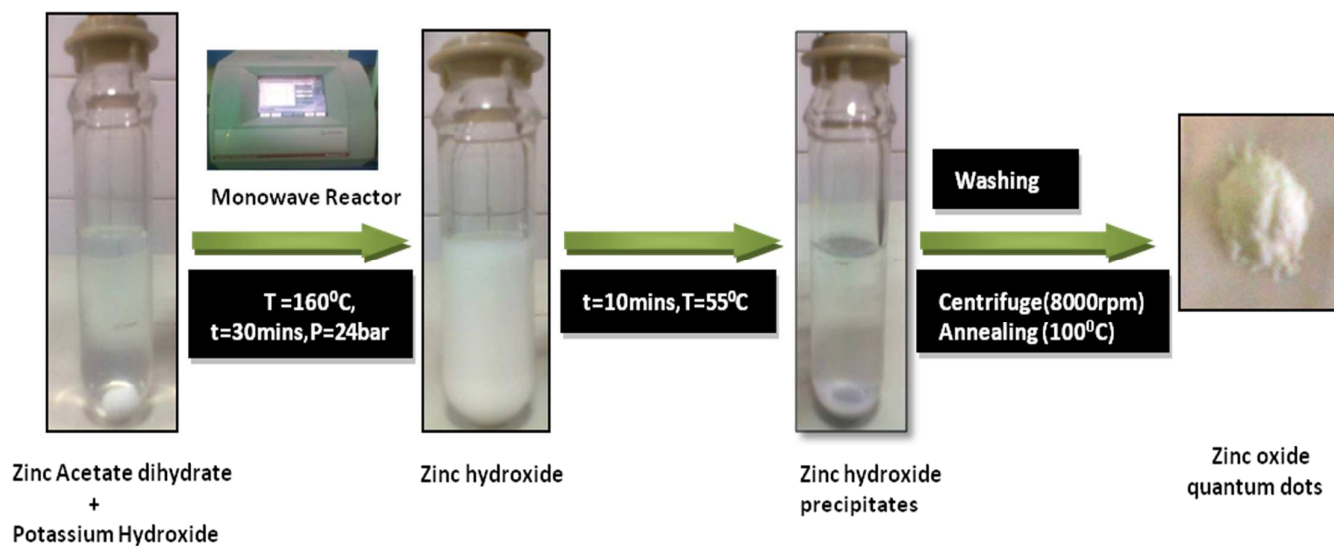


Figure 1: The ZnO nanoparticle synthesis process flow.

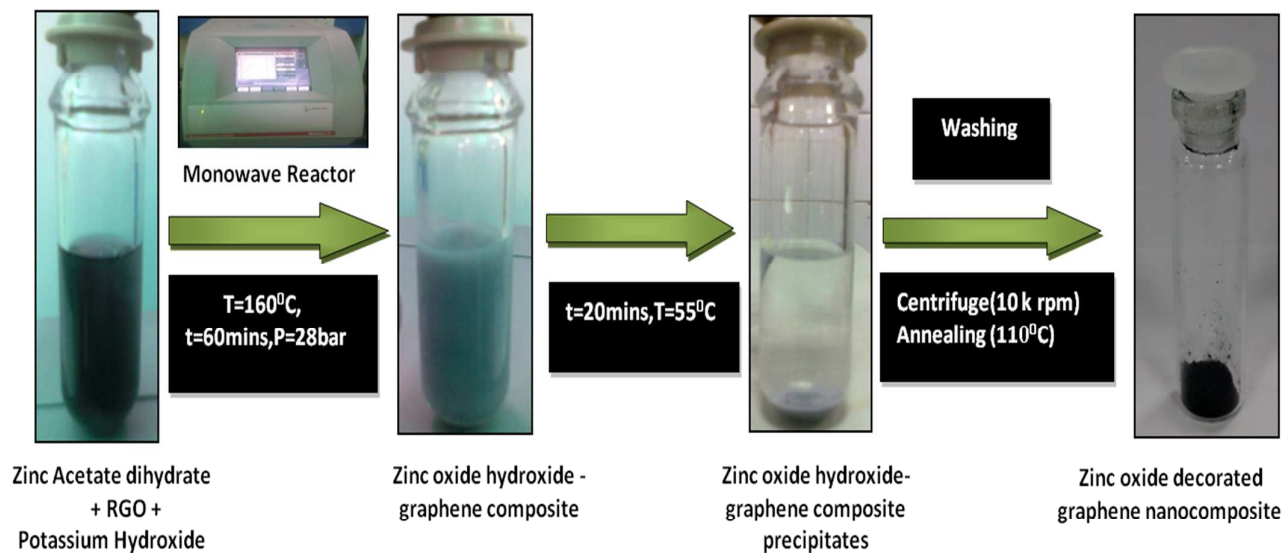


Figure 2: The ZnO nanoparticles decorated graphene nanocomposite synthesis process flow.

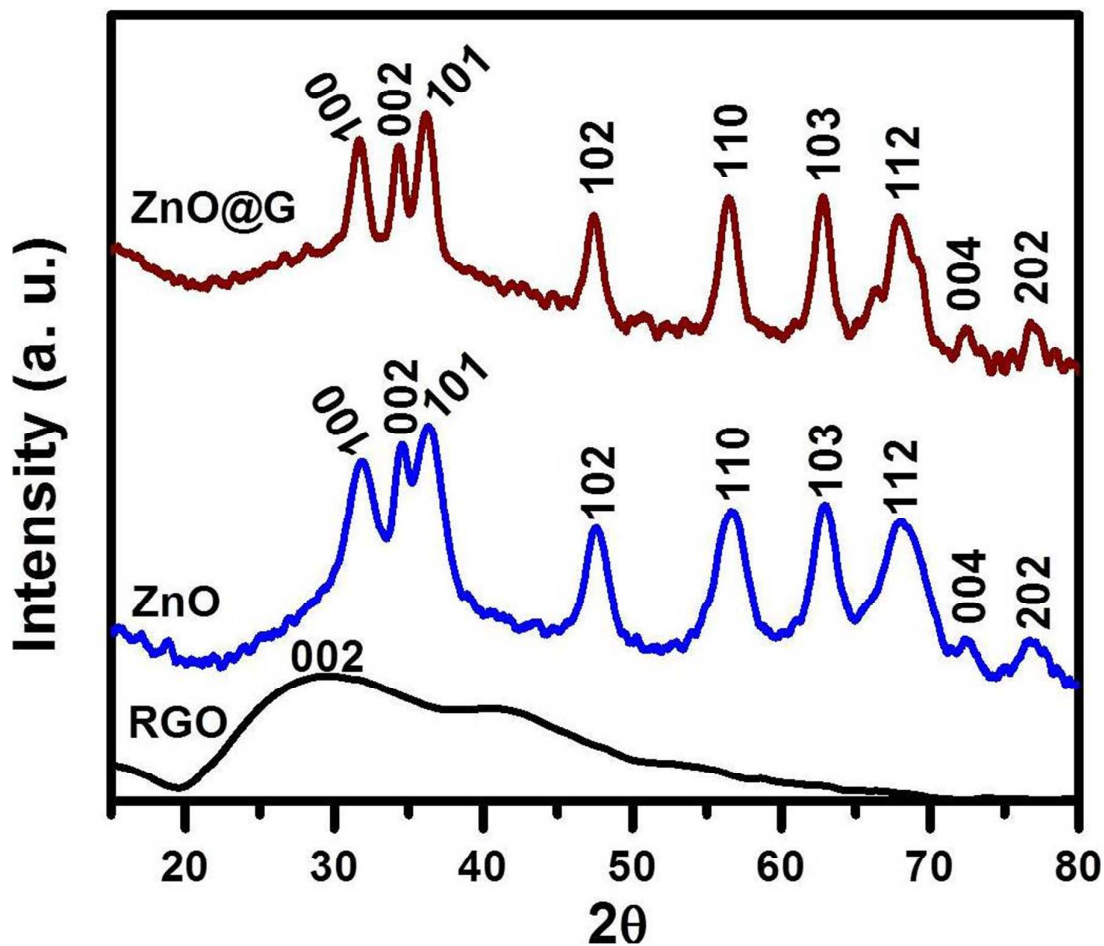


Figure 3 : The XRD intensities for reduced Graphene oxide (RGO), ZnO nanoparticles (ZnO) and ZnO-Graphene nanocomposite (Z@G) described phase and crystallinity of ZnO and RGO along with interlayer effect in hybrid or composite.

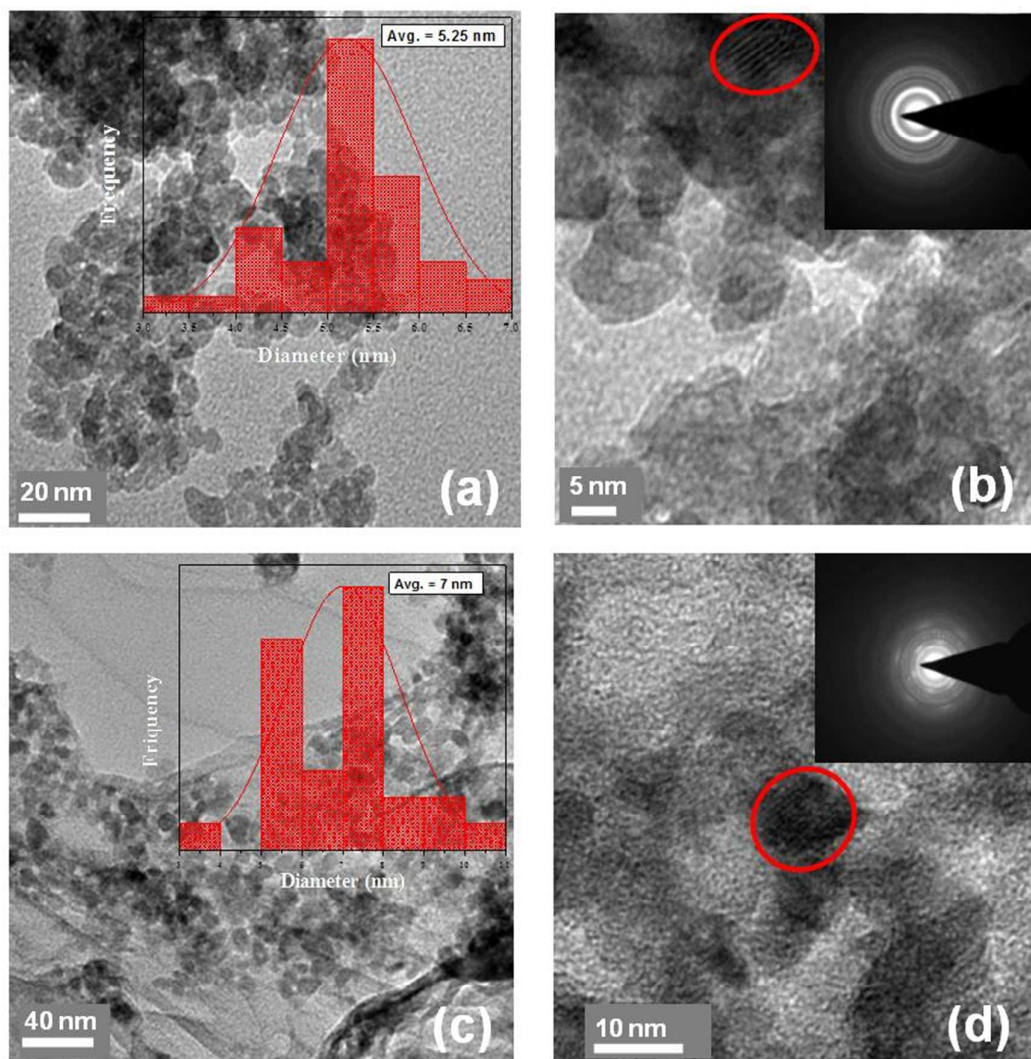


Figure 4 : The HRTEM image of (a) ZnO nanoparticles; and (c) ZnO-Graphene nanocomposite (Z@G); with average particle size 5.25 nm and 7 nm; and highly resolved images (b) and (d) with SAED pattern in the inset featuring highly crystalline ZnO structure indexed as hexagonal wurtzite phase and polycrystalline nature of Z@G nanocomposite, respectively.

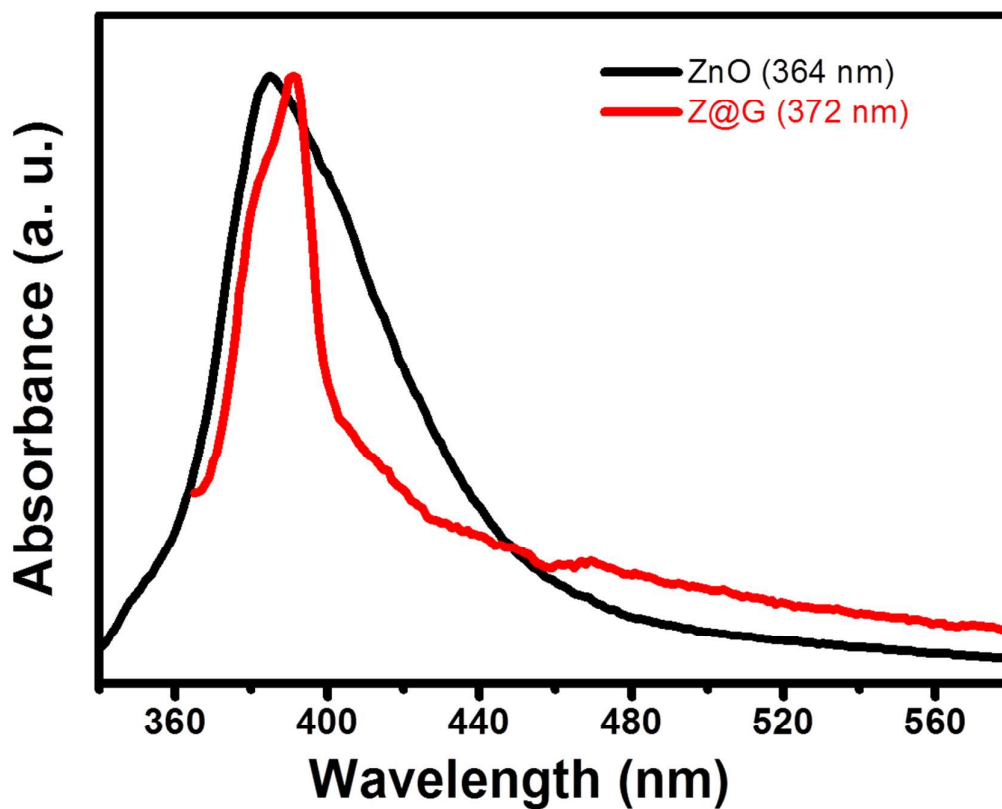


Figure 5 : The normalized UV-Vis spectra of as synthesized ZnO nanoparticles and Z@G nanocomposite with strong absorption peak at 364 nm and 372 nm, respectively, ensuring modified absorption.

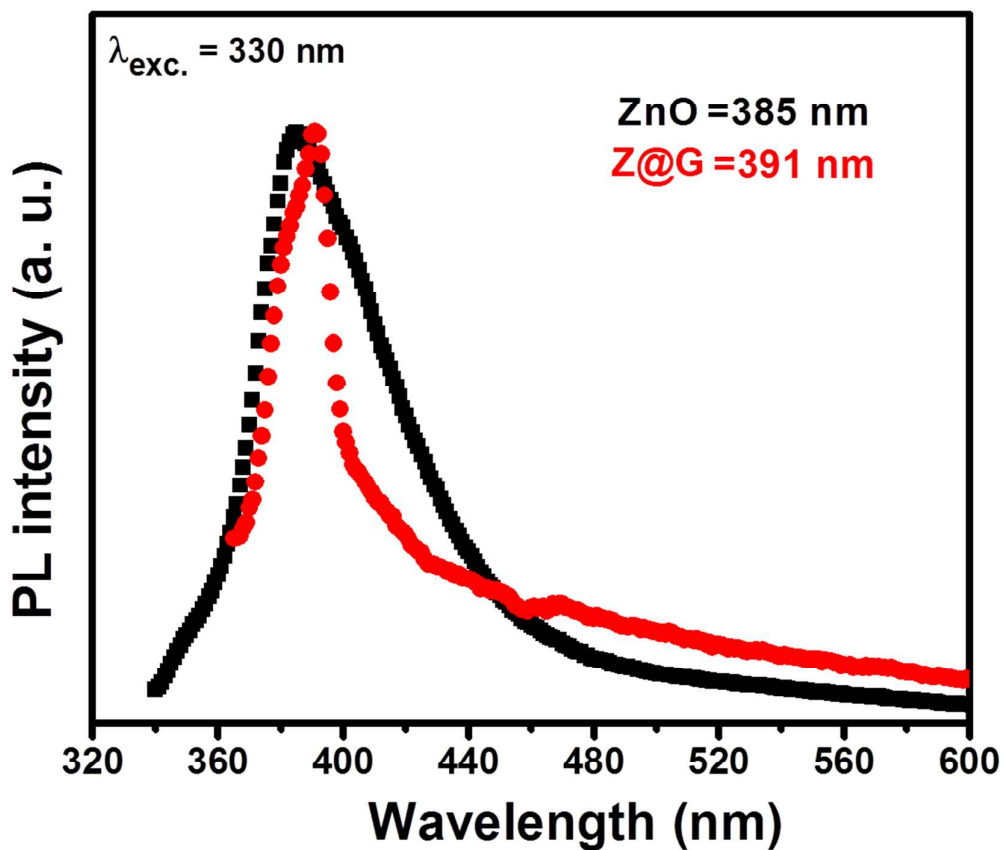


Figure 6 : The normalized PL spectra of as synthesized ZnO nanoparticles and Z@G nanocomposite with strong UV emission band peak at 385 nm and 391 nm, respectively, in response to excitation at 330 nm produces a red shift that signify the interaction and coupling between ZnO nanoparticles and Graphene.

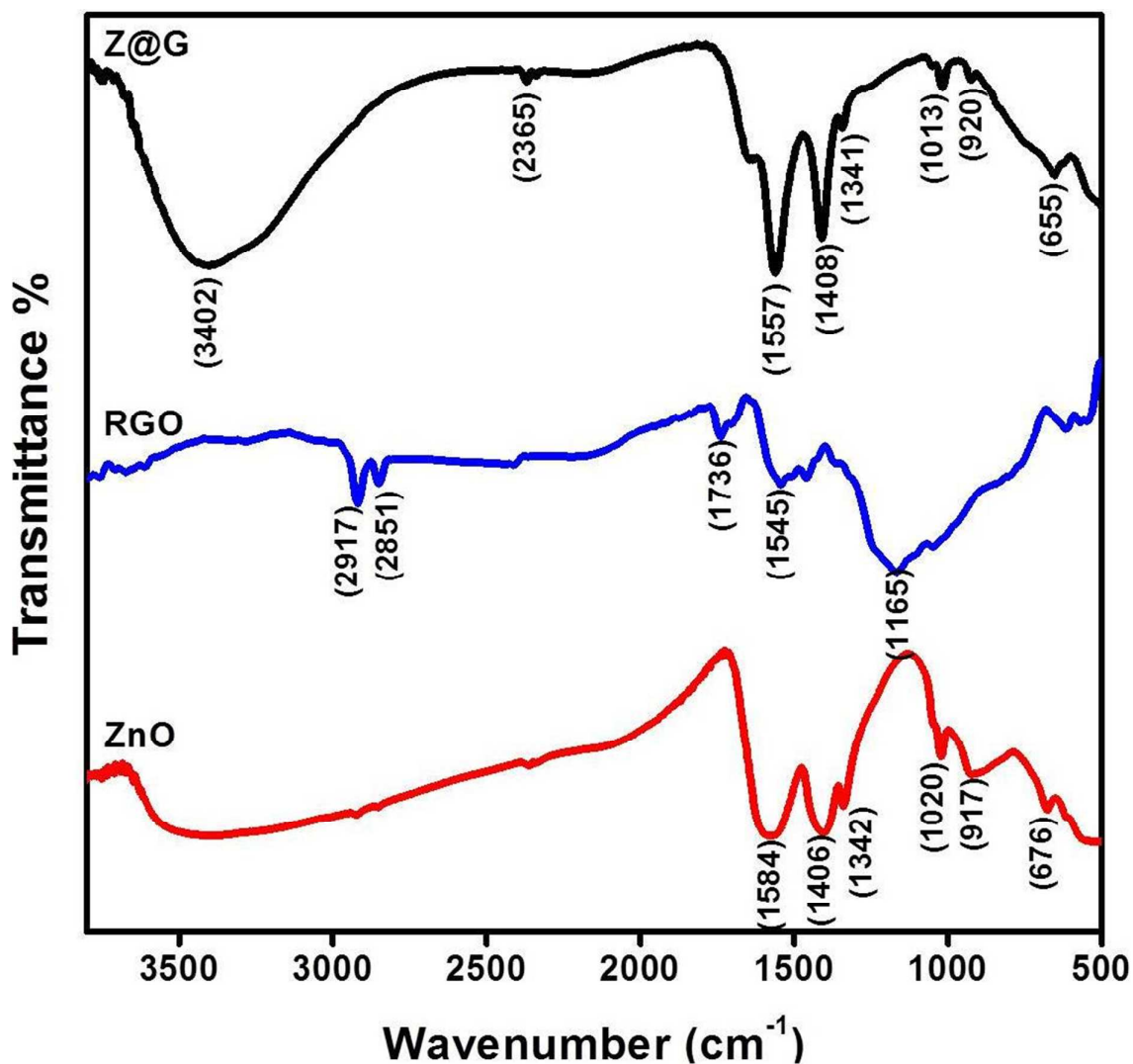


Figure 7 : The FTIR spectra of ZnO nanoparticles reduced Graphene oxide (RGO) and Z@G nanocomposite informing on attached functional groups and chemical changes with anchoring of ZnO nanoparticles at Graphene nanosheets.

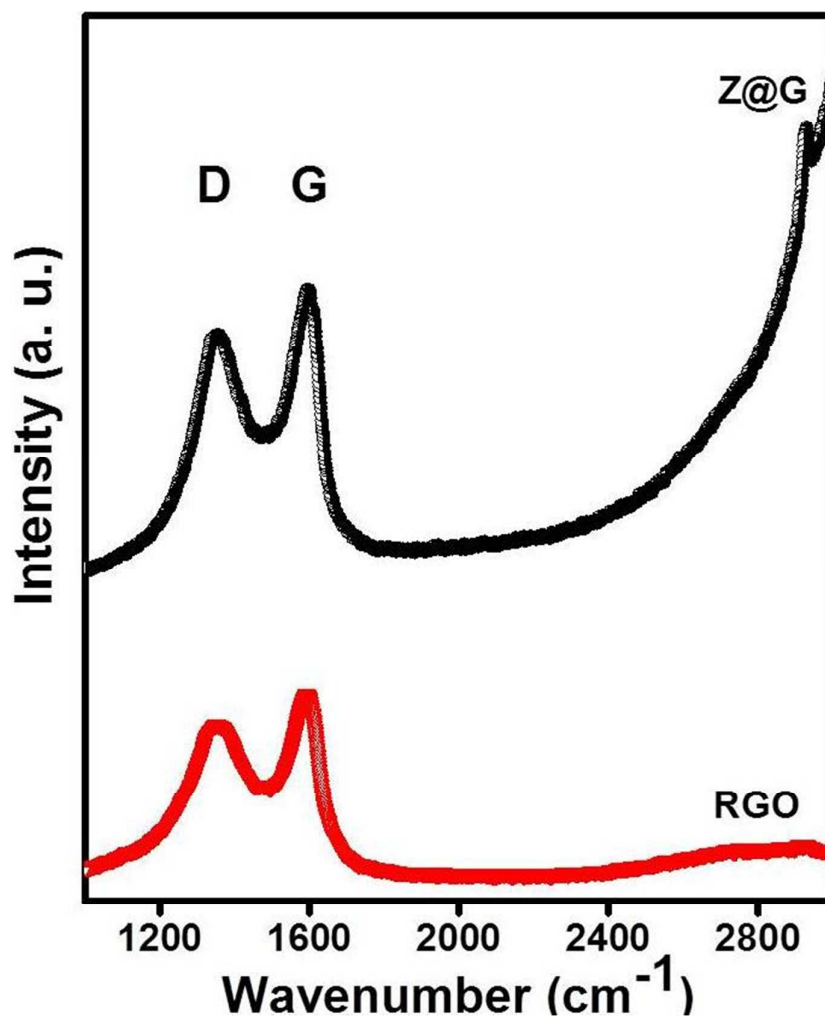


Figure 8 : The Raman spectra of RGO and Z@G nanocomposite shows blue shift (D-band) and red shift (G-band) and low intensity ratio (I_D/I_G) point out interaction between ZnO and Graphene and less defective composition of Z@G, respectively.

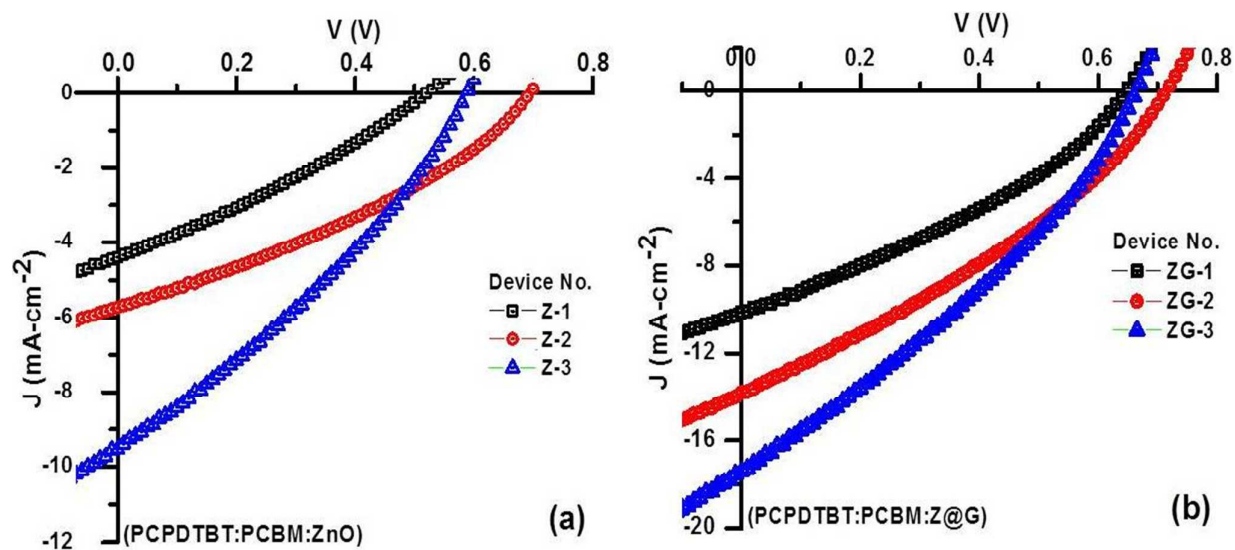


Figure 9 : The J-V characteristics of the solar cell devices based on active layer (a) PCPDTBT: PCBM: ZnO nanoparticles {Z-1, Z-2 & Z-3}; and (b) PCPDTBT: PCBM: Z@G nanocomposite {ZG-1, ZG-2 & ZG-3}; with overall concentration 30 and 40 mg/ml and different weight ratios as 1:1:1 & 1:1:2, respectively.

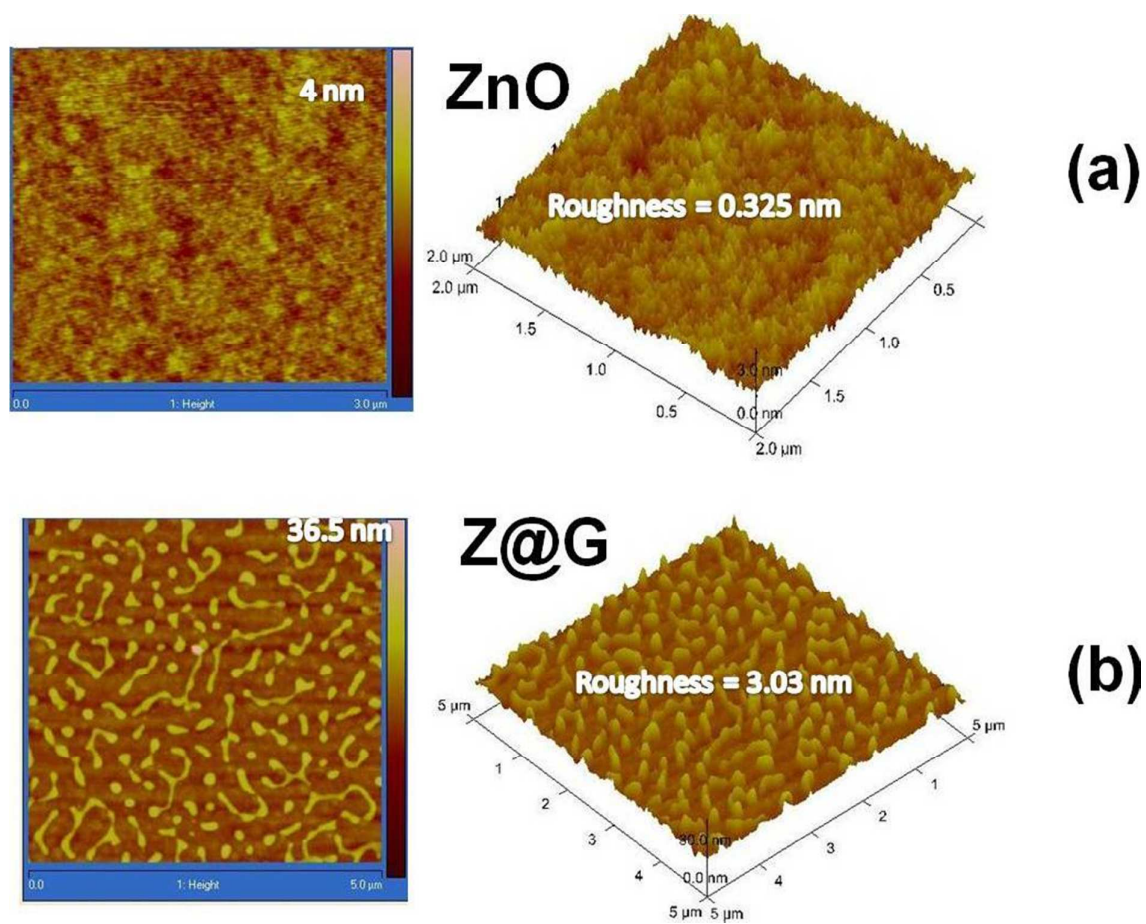


Figure 10 : The AFM micrograph of thin film of (a) PCPDTBT:PCBM: ZnO nanoparticles; and (b) PCPDTBT:PCBM: Z@G nanocomposite with roughness 0.32 and 3.03 nm, respectively.

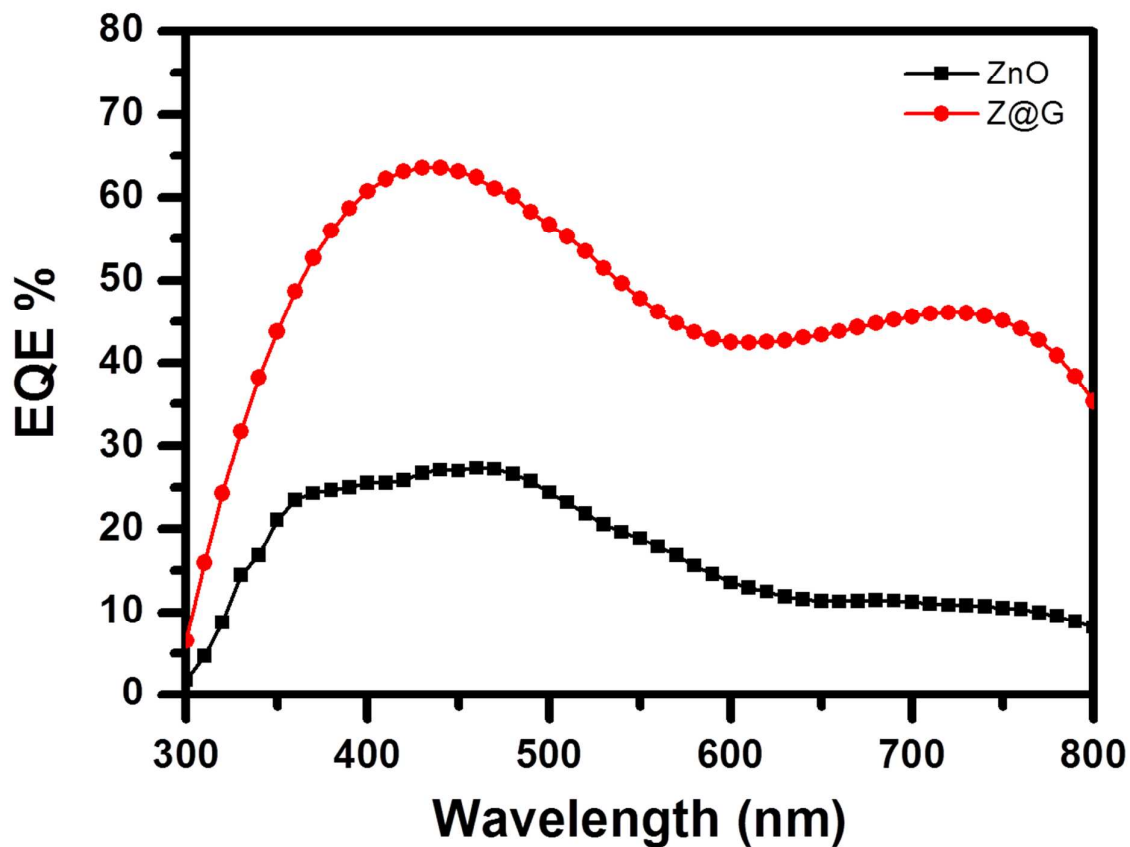


Figure 11 : External quantum efficiency of PCPDTBT: PCBM: ZnO nanoparticles and PCPDTBT: PCBM: Z@G nanocomposite based devices respectively.

Table:

Table 1 : Hybrid solar cell performances (ITO/PEDOT:PSS/PCPDTBT:PCBM:ZnO or Z@G /Al) with varied active layer concentration and weight ratios of organic blend (PCPDTBT: PCBM) and inorganic nanostructures (ZnO or Z@G), respectively.

Device Architecture		Weight ratio	Device No.	J_{sc} ($\text{mA}\cdot\text{cm}^{-2}$)	V_{oc} (V)	FF (%)	η (%)	R_s ($\Omega\cdot\text{cm}^2$)	R_{sh} ($\Omega\cdot\text{cm}^2$)
ITO/PEDOT:PSS/ PCPDTBT:PCBM:ZnO /Al	30	1:1:1	Z-1	4.40	0.52	30	0.68	77	168
	40	1:1:2	Z-2	5.72	0.69	34	1.34	49	200
	40	1:1:1	Z-3	9.53	0.59	31	1.76	30	96
ITO/PEDOT:PSS/ PCPDTBT:PCBM:Z@G /Al	30	1:1:1	ZG-1	10.12	0.65	33	2.16	26	107
	40	1:1:2	ZG-2	13.63	0.71	33	3.18	23	82
	40	1:1:1	ZG-3	17.45	0.66	32	3.65	18	60

Graphical abstract

Graphene assisted charge transportation doubles the power conversion efficiency of PCPDTBT:PCBM:ZnO based bulk heterojunction solar cells.

